Local Connected Fractal Dimensions and Lacunarity Analyses of 60° Fluorescein Angiograms

Gabriel Landini, Philip I. Murray,† and Gary P. Misson†*

Purpose. The retinal vascular tree exhibits fractal characteristics. These findings relate to the mechanisms involved in the vascularization process and to the objective morphologic characterization of retinal vessels using fractal analysis. Although normal retinas show uniform patterns of blood vessels, in pathologic retinas with central vein or artery occlusions, the patterns are irregular. Because the generalized box fractal dimension fails to differentiate successfully between normal and abnormal retinal vessels in 60° fluorescein angiograms, the authors have further investigated this problem using the local connected fractal dimension (α).

Methods. The authors studied 24 digitized 60° fluorescein angiograms of patients with normal retinas and 5 angiograms of patients with central retinal vein or artery occlusion. The pointwise method estimated the local complexity of the angiogram within a finite window centered on those pixels that belong to the retinal vessels. Color-coded dimensional images of the angiograms were constructed by plotting the pixels forming the object with a color that corresponded to specific values of $\alpha \pm \Delta\alpha$.

Results. The color-coded representation allowed recognition of areas with increased or decreased local angiogram complexity. The α distributions showed differences between normal and pathologic retinas, which overcomes problems encountered when using the methods of calculating the generalized fractal dimensions. A multivariate linear discriminant function using parameters from the α distribution and a further fractal parameter—lacunarity—reclassified 23 of the 24 normal and 4 of the 5 pathologic angiograms in their original groups (total: 92.1% correct).

Conclusions. This methodology may be used for automatic detection and objective characterization of local retinal vessel abnormalities. Invest Ophthalmol Vis Sci. 1995;36:2749–2755.

Fractals are geometric objects whose increasing details under magnification resemble exactly or statistically the whole object (self-similarity). Such fractal objects are not easily "measurable" in classic geometric terms because some of their physical characteristics (length, mass, area, volume, and so on) are largely dependent on the magnification used when they are measured. Normal retinal vasculature is statistically self-similar within a range of scales; therefore, it can be considered fractal.[2–14] Its degree of complexity (self-similarity) can be expressed by a single fractional number, the fractal dimension (D).

*From the *Oral Pathology Unit, School of Dentistry, and the †Academic Unit of Ophthalmology, The University of Birmingham, United Kingdom.*
Supported by the British Council for the Prevention of Blindness.
Submitted for publication May 8, 1995; revised June 20, 1995; accepted August 21, 1995.
Proprietary interest category: N.
Reprint requests: Gabriel Landini, Oral Pathology Unit, School of Dentistry, The University of Birmingham, St. Chad's Queensway, Birmingham B4 6NN, United Kingdom.

Figure 1 shows a fractal object: a computer-generated cluster produced by a stochastic growth model based on diffusion termed diffusion-limited aggregation, or DLA. Some properties of the cluster include self-similarity (small branches of the cluster are statistically indistinguishable from large ones when the observational scale changes) and absence of defined density; sampling the object at different resolutions (using different sample sizes) gives different results. For this type of object, one can instead look at the *variation* in some physical property, such as space filling or mass, *with change of scale.* Fractal analysis quantifies this variation using multiresolution methods and provides a new way of characterizing the object in terms of a fractal dimension. Two common methods of fractal analysis are the *box counting method* and the *mass-radius relation.* The box counting dimension is computed by superimposing on the object a grid of size ϵ, counting how many boxes $N(\epsilon)$ contain the object, and re-

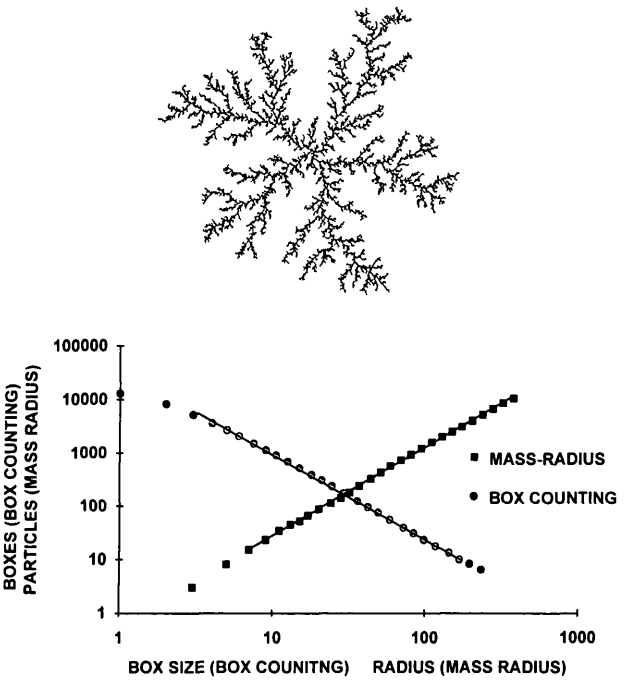

FIGURE 1. A computer-generated fractal cluster produced by the diffusion limited aggregation model. The graph shows the procedure for estimating the box counting dimension by plotting (*open circles*) the logarithm of the number of boxes of size ϵ needed to cover the cluster versus the logarithm of ϵ. The slope of the plot (linear regression) is -1.64; therefore, D_{box} for this cluster is 1.64. The mass–radius relation is found by plotting (*filled squares*) the logarithm of the number of cluster particles within a circle of radius r versus the logarithm of r. The slope of the line is 1.66 and $D_{mass-radius} = 1.66$. Note that these dimensional values are larger than that of a line ($D = 1$) and smaller than that of a plane ($D = 2$).

peating the task for various box sizes ϵ. Plotting the logarithm of number of boxes $N(\epsilon)$ versus the logarithm of ϵ produces a straight line with slope $-D$, where D is the box fractal dimension. In this way, an estimation is obtained of the change in space filling with change of observational scale: a filled plane gives $D = 2$, a line $D = 1$, a point $D = 0$, and fractals on the plane have fractional values $0 \leq D \leq 2$ (Fig. 1). Another way to estimate a fractal dimension is by the mass–radius relationship: The procedure is to measure the increase of mass $M(r)$ in the object within circles of increasingly sized radii r centered at a particular point of the object (most often the center of gravity). Again, for a fractal object, the log–log plot of $M(r)$ versus r is a straight line, this time with slope D. This value of D_1, instead of being an integer value, is fractional; for example, filled objects embedded in the plane, such as filled squares and circles, have an increase of "mass" proportional to the *square* of the radius (exponent 2 and thus $D = 2$). Both approaches give similar dimensional values (Fig. 1), but they express different attributes of the object. Although the box dimension is quantification of the space filling, the mass radius relation is a pointwise measure relative to an arbitrary center point (this assumes some form of rotational symmetry in the object). However, the fractal dimension alone does not describe fractal objects fully. Highly dissimilar patterns may have the same fractal dimension or may be multifractal (the geometric characteristics are expressed by a spectrum of fractal dimensions). In those cases, a single D value is not enough for characterization, and other approaches such as the lacunarity parameter[1,15–18] or multifractal spectrum analysis[19,20] must be used. We previously determined the generalized fractal dimensions for normal retinas using the box counting algorithm in 60° fluorescein angiograms,[8,10] whereas several other groups have investigated the box dimension of photomontages,[9,13] mass–radius relationship, and the two-point correlation function,[2–7,11,12,14] in various photographic projections and in preselected and localized areas of interest.[12,14] Although 60° angiograms show uniform patterns of blood vessels, in pathologic cases, such as retinal venous or arterial occlusions, the patterns look irregular. Unfortunately, the generalized box fractal dimension fails to differentiate successfully between the retinal vessel patterns found in normal retinas and in vascular occlusions[8] as D is an overall or an average measure, and most of the occlusion angiograms show locally low-dimensional areas caused by nonfilling of vessels together with locally high-dimensional areas caused by increased (collateral) circulation. We have further investigated this problem using the concept of local connected fractal dimension.

METHODS

The methodology was implemented by one of the authors (GL) to achieve a semiautomatic procedure, and it involved the following stages: image collection, digitization, and fractal analysis.

Image Collection

The study material consisted of fundus fluorescein angiograms from 24 patients with no ophthalmic disease, four patients with central retinal vein occlusion, and one patient with a central retinal artery occlusion, all taken with a 60° Topcon (Tokyo, Japan) TRC 50VT fundus camera. Informed consent was obtained from each patient. The tenets of the Declaration of Helsinki were followed, and institutional human experimentation committee approval was granted. The angiograms were projected onto paper and hand traced at high magnification and constant thickness down to vessels of approximately 40 μm in diameter (the size limit to which the vessels throughout the fundus could be

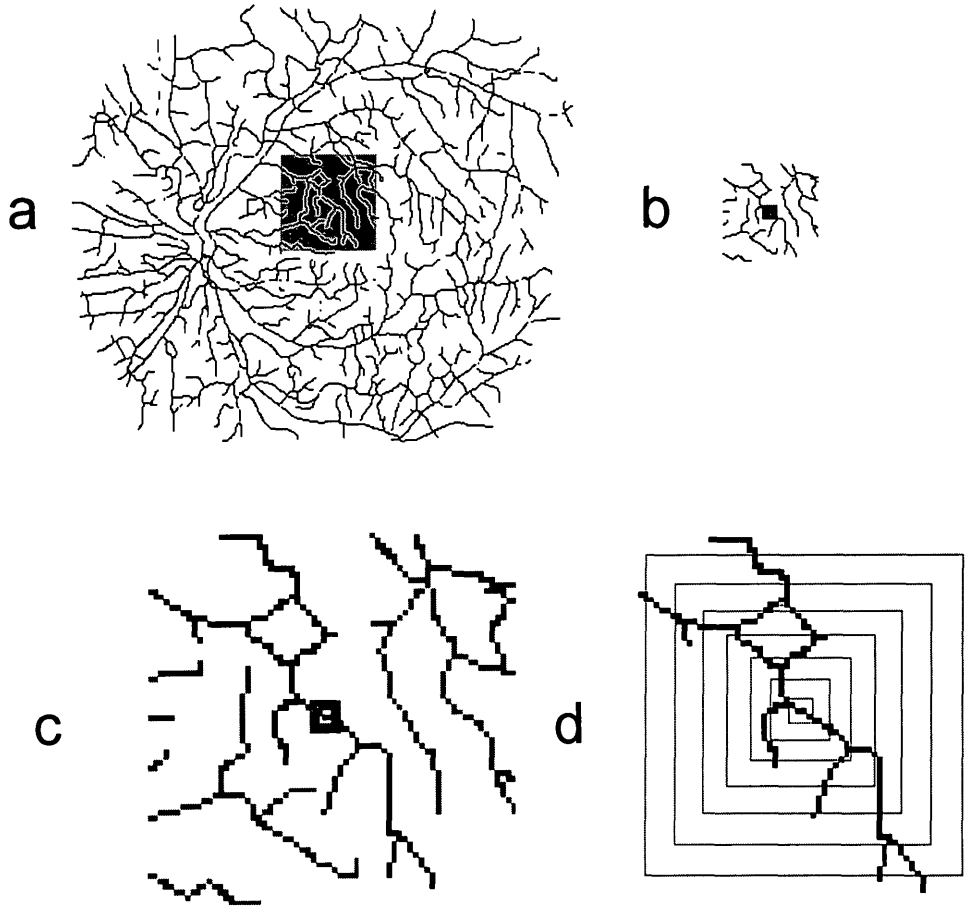

FIGURE 2. Diagrammatic representation of the method used to estimate the local connected fractal dimension of the angiograms. (**A**). A digitized version of an angiogram with a window of 31 × 31 pixels centered at a particular pixel *P*. (**B**) The set within the window is isolated (the dark square marks *P*, the center of the window). (**c**) The local connected set *S* is shown in black, whereas nonconnected pixels are gray. (**D**) The analysis of the number of pixels in *S* within increasingly sized boxes, centered at *P*.

traced accurately and consistently in our photographs). The arterial and venous trees were traced in combination, and the traced angiograms always included the optic disc and macular areas.

Digitization

Tracings were digitized as binary images in a computer with square pixels using an image scanner (OMRON, Tokyo, Japan). The scanned image had a resolution of 1 pixel (1 pixel = 33.46 μm), and the angiograms consisted of approximately 400 × 400 pixels. The scanned images were reduced to a single pixel width (skeletonized) to avoid the effects of the thickness of the tracings because the interest was in the spatial distribution of the vessels, not in vessel thickness.

Fractal Analysis

The binary images were analyzed by estimating their local mass scaling properties, that is, the increase of mass (number of pixels forming the image of the blood vessels) within an increasingly sized mask. As the angiograms were represented by 1-pixel-thick clusters, the computer program measured the total number of pixels local connected in a box of increasing size ϵ centered at a point x,y.[21] In this context, "local connected" relates to all the pixels within the largest box used for the analysis (31 pixels) that belong to the cluster connected to the pixel on which the box is centered (Fig. 2). This method was applied to all the pixels belonging to the retinal vascular tree. The scaling relation is found by the linear regression (least squares) of the logarithm of the mass (pixels) in a box of size ϵ on the logarithm of ϵ. The relationship is expressed as

$$M(\epsilon) \propto F\epsilon^{\alpha} \quad (1)$$

and

$$\alpha = \frac{\log[M(\epsilon)]}{\log(\epsilon)} \quad (2)$$

TABLE 1. Local Connected Dimension Values From Test Fractal Objects

Object	*Analytical D*	*Mean α ± SD*	*% Error From D*	*Mode α*	*αs Analysed*
Circle	1.00000	1.0000 ± 0.0000	0.000	1.00	1696
Koch 1	1.12915	1.1626 ± 0.0404	2.877	1.18	3840
Koch 2	1.26186	1.2651 ± 0.0506	0.256	1.26	6043
Koch 3	1.36521	1.3361 ± 0.0623	−2.179	1.31	11771
Koch 4	1.50000	1.4898 ± 0.0752	−0.685	1.50	22820
Koch 5	1.55105	1.5065 ± 0.1134	−2.957	1.50	35942
Koch 6	1.66667	1.7060 ± 0.1063	2.306	1.79	50098
Sierpinski carpet	1.89279	1.8402 ± 0.0792	−2.858	1.89	32768
Plane	2.00000	2.0000 ± 0.0000	0.000	2.00	9118

SD = standard deviation; D = generalized fractal dimension.

where $M(\epsilon)$ is the number of local connected pixels (eight-neighborhood connection) in a box of side size ϵ, F is a mass pre-factor, and α is the exponent characterizing the relationship.[21] If the object is a completely filled area, the object is two dimensional and $\alpha = 2$; if it is a straight line (one dimensional), then $\alpha = 1$ and values in between describe the local complexity of the set (the local connected fractal dimension). Although α has similarities to the fractal dimension (estimated using, for example, the mass–radius relation), its value for sets embedded in two dimensions can take values <1 or >2. The size of ϵ_{max} was 31 pixels, which corresponded to approximately 1037 μm in the retina. The procedure is as follows and is graphically summarized in Figure 2:

For every pixel that "belongs" to a blood vessel in the angiogram:

1. Call the current pixel P.
2. Find all the pixels connected to P within a 31 pixel-side window centered at P (this is the "local connected set" S).
3. Count the number of pixels $M(\epsilon)$ of S, in boxes of increasing side size ϵ ($1 \leq \epsilon \leq 31$) centered at P.
4. Calculate the local connected fractal dimension of S relative to P using equation *2* by linear regression of *log(M(ε))* versus *log(ε)*. The regression formula $y = a + bx$ gives the parameters of equation *1*: a = mass prefactor F, and b = local connected fractal dimension α.

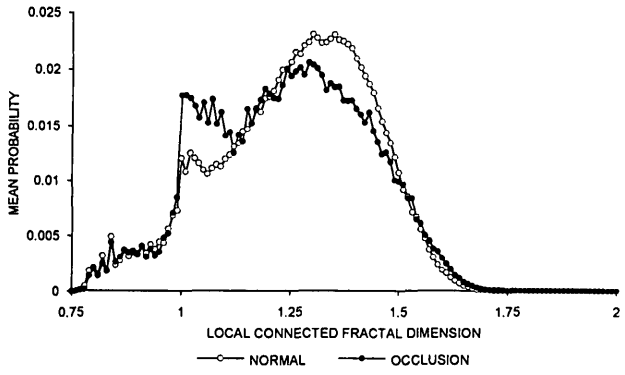

FIGURE 3. Mean distribution of α values for the normal and occlusion angiograms. Note that the pathologic cases have a higher probability of low-dimensional features (near $\alpha \sim$ 1.00 to 1.10 region) that corresponds to the areas devoid of blood vessels (the artery–vein occlusion area) and a larger tail of the distribution toward high αs (hyperemic area) that occur through a reduction of the peak seen between 1.25 and 1.5, representing the range of values for local connected fractal dimension for the normal cases.

The α values were rounded to two significant fractional digits, and, subsequently, the average α, median α, and mode α were calculated. A further parameter called *lacunarity* Λ (lacuna is Latin for *gap*) that is a measure of the texture of fractals was calculated as the discrepancy in the expected value of $\overline{F}$ (the mean F)[1,15] using the second-order expression proposed by Mandelbrot[1]:

$$\Lambda = \overline{\left(\frac{F}{\overline{F}} - 1\right)^2} \qquad (3)$$

where the horizontal lines mean average. Note that where F and $\overline{F}$ are equal, $\Lambda = 0$. Several other definitions of lacunarity have been suggested.[16–19]

RESULTS

The methods were validated using a series of geometric fractals with analytically determined fractal dimension (the method had mean error of −0.36% ± 2.08 for the mean α of all the test patterns used) (Table 1), and the consistency of the traced angiograms has been reported elsewhere.[10] The total number of αs for all cases was 268,599, with a mean of 9262 ± 1876 per case. The mean distribution probability and the variance of αs per bin in the normal and pathologic

TABLE 2. Summary of the Parameters From the Local Connected Fractal Dimension and Lacunarity Analyses for the Whole Angiogram

Parameter	*Normal Patients*	*SD*	*Patients With Occlusion*	*SD*	*t-test* P	*F-test* P
Mean α*	1.2594	0.0283	1.2414	0.0644	0.0967	0.0079
Median α*	1.2775	0.0322	1.2520	0.0695	0.0807	0.0029
Mode α*	1.3283	0.0524	1.1980	0.1550	0.0002	0.0004
Minimum α	0.7704	0.0130	0.7780	0.0110	0.0014	0.8112
Maximum α	1.6988	0.0460	1.6800	0.0822	0.1657	0.0638
Lacunarity*	2.8984	1.0912	7.6239	10.375	0.0119	0.0000

SD = standard deviation.
* Parameters used in the linear discriminant function (see Table 3).

groups are shown in Figures 3 and 4. The mean values of the mean, median, mode, minimum, and maximum α and Λ in the normal and occlusion angiograms, as well as the probability for the Student's *t*-test and F-test, are shown in Table 2. None of the variables individually allowed a useful discrimination between the two groups (the mode, minimum α, and lacunarity using the *t*-test were significantly different between the groups for $P < 0.05$, but there was data overlap). F-tests for variability of the variances were significantly different for the mean, median, mode, and lacunarity, and these variables were used in a multivariate linear discriminant function to investigate any association that could lead to a classifier. The discriminant analysis successfully reclassified 27 of the 29 (92.1%) angiograms correctly in the original groups (one normal and one vein occlusion were wrongly classified) (Table 3). Other parameters such as the generalized box dimension[10] entropy of the distribution of αs,[22] maximum α, and minimum α also were investigated, but they did not introduce any advantages in the analysis (entropy, maximum α) or introduce confusion, reducing the discrimination rate (minimum α, box dimension).

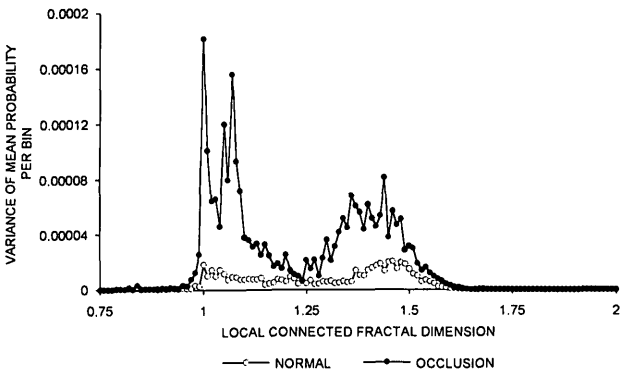

FIGURE 4. Variance of the mean α distribution in normal and occlusion cases. Note the large peaks in the occlusion cases, revealing higher variability of the low- and high-dimensional features of the angiograms.

Because every local connected fractal dimension is associated with a single pixel, this fact can be used to produce a dimensional mapping on the original angiogram by setting each pixel of the angiogram to a color that corresponds to a particular value of α following a reference (look-up) table. This approach may be suitable for unbiased isolation of areas with blood vessels of abnormal architecture (Fig. 5) or for image enhancement of those areas.

DISCUSSION

The objective characterization of the architecture of the retinal vascular tree is a difficult task because of the geometric complexity of the blood vessels and the lack of a morphologic model that could describe it. Consequently, angiogram analysis has remained an expert activity that nevertheless has a subjective component yielding to interobserver and intraobserver variation. The development of fractal geometry, however, has allowed the formal understanding of many natural mechanisms and patterns that were considered "random" or "complex." It also has given new models of pattern formation that may play fundamental roles in the process of vasculogenesis, such as diffusion-limited aggregation (a model of stochastic growth

TABLE 3. Summary of Classification of the Patients Into the Original Groups Using a Multivariate Linear Discriminant Function Analysis

	True Groups	
Put Into Group	*Normal*	*Occlusion*
Normal	23	1
Occlusion	1	4
Total *N*	24	5
N correct	23	4
Proportion	0.958	0.800

FIGURE 5. A vein occlusion angiogram and a thresholded version of the dimensional map showing only pixels with $\alpha > 1.45$. Note that the hyperemic area can be detected easily (*top right*). This procedure may be used to enhance the image with color coding or to isolate locations automatically with specific characteristics based on their complexity.

in Laplacian diffusion fields)[23] and self-avoiding invasion percolation (a model of diffusion in disordered media).[7]

We have used a morphologic approach based on fractal geometry to produce an objective method for assessment of 60° angiograms. Our previous data[10] on 60° fluorescein angiograms of normal retinas revealed a fractal box dimension (D) of 1.76 ± 0.02 for arteries and veins combined. At that time, it was proposed that retinas with vasculopathies may have different values of D and that fractal analysis may be of diagnostic value. Further analysis revealed that this was not necessarily the case.[8] Although D is an "average" measure of complexity that describes the global features of the object, there are localized morphologic changes that (at least for the cases analyzed) masked each other. For example, retinas with vein occlusion have areas depleted of blood vessels (with lower D), whereas in other locations there is a compensatory increase in blood vessels (yielding a higher D). This can be seen as a local maxima in the vicinity of $\alpha \sim 1$ (more linear features) and a slightly longer tail (more complex features) toward the high values of α in the mean α frequency of the occlusion cases compared to the normal (Fig. 3). These variations also produce the higher variances of the mean α frequency in Figure 4. Note that the highest variances are again in the low (α near 1) and high (α near 1.5) parts of the spectrum of αs. When these characteristics are not considered and a single fractal dimension D is estimated, because D is a global value, these small changes may go unnoticed. The solution to this problem can be tackled from two points of view. Either preselect the region of interest to analyze (which has been proven useful for the monitoring of treatment in specific locations[11,12]) or characterize the entire angiogram based on local dimension analysis as described in this article. One advantage of our approach is that it also may be used to preselect automatically the area of interest by means of the dimensional mapping onto the angiogram (for example, thresholding for αs larger or smaller than average).

The results of the multivariate discriminant function analysis may appear elementary because the vascular architecture appears evident to expert observers; however, the methodology is unbiased and reproducible, and it does not require human intervention. Therefore, it may be invaluable for inspecting or monitoring massive numbers of patients if there is a lack of expert personnel, time, or resources. The combination of the described methodology with automatic vessel segmentation algorithms is under investigation.

Key Words

central vein occlusion, fractal, image analysis, morphometry, retinal vasculature

References

1. Mandelbrot BB. *The Fractal Geometry of Nature.* San Francisco: Freeman; 1982.
2. Masters BR, Platt DE. Development of human retinal vessels: A fractal analysis. ARVO Abstracts. *Invest Ophthalmol Vis Sci.* 1989;30:391.
3. Masters BR, Family F, Platt DE. Fractal analysis of human retinal vessels. *Biophys J.* 1989;55:575a.
4. Family F, Masters BR, Platt DE. Fractal pattern formation in human retinal vessels. *Physica D.* 1989;38:98–103.
5. Masters BR. Fractal analysis of human retinal blood vessels patterns: Developmental and diagnostic aspects. In: Masters BR, ed. *Noninvasive Diagnostic Techniques in Ophthalmology,* New York: Springer Verlag; 1990:515–527.
6. Mainster MA. The fractal properties of retinal vessels: Embryological and clinical implications. *Eye.* 1990;4:235–241.
7. Daxer A. Fractals and retinal vessels. *Lancet.* 1992;339:618. Letter.
8. Misson GP, Landini G, Murray PI. Fractals and ophthalmology. *Lancet.* 1992;339:872. Letter.

9. Masters BR, Sernetz M, Wlczek P. Image analysis of human retinal blood vessels and their characterization as fractals. *Acta Stereol.* 1992;11(suppl 1):355–360.
10. Landini G, Misson GP, Murray PI. Fractal analysis of the normal human retinal fluorescein angiogram. *Curr Eye Res.* 1993;12:23–27.
11. Daxer A. The fractal geometry of proliferative diabetic retinopathy: Implications for the diagnosis and the process of retinal vasculogenesis. *Curr Eye Res.* 1993;12:1103–1109.
12. Daxer A. Characterisation of the neovascularisation process in diabetic retinopathy by means of fractal geometry: Diagnostic implications. *Graefe's Arch Clin Exp Ophthalmol.* 1993;231:681–686.
13. Masters BR. Fractal analysis of normal human retinal blood vessels. *Fractals.* 1994;2:103–110.
14. Daxer A. Mechanisms in retinal vasculogenesis: An analysis of the spatial branching site correlation. *Curr Eye Res.* 1995;14:251–254.
15. Obert M. Numerical estimates of the fractal dimension D and the lacunarity L by the mass radius relation. *Fractals.* 1993;1:711–721.
16. Voss RF. Fractals in nature: From characterization to simulation. In: Peitgen H–O, Saupe D, eds. *The Science of Fractal Images.* New York: Springer Verlag; 1988.
17. Mandelbrot BB. A fractal's lacunarity, and how it can be tuned and measured. In: Nonnenmacher TF, Losa, GA, Weibel ER, eds. *Fractals in Biology and Medicine.* Basel: Birkhauser Verlag; 1994:8–21.
18. Allain C, Cloitre M. Characterizing the lacunarity of random and deterministic fractal sets. *Phys Rev A.* 1991;44:3552–3558.
19. Hasley TC, Jensen MH, Kadanoff LP, Procaccia I, Shraiman BI. Fractal measures and their singularities: The characterization of strange sets. *Phys Rev A.* 1986;33:1141–1151.
20. Meneveau C, Sreenivasan KR. Measurement of f(α) from scaling of histograms, and applications to dynamical systems and fully developed turbulence. *Phys Lett A.* 1989;137:103–112.
21. Voss RF, Wyatt JCY. Multifractals and the local connected fractal dimension: Classification of early Chinese landscape paintings. In: Crilly T, Earnshaw RA, Jones H, eds. *Applications of Fractals and Chaos.* Berlin: Springer Verlag; 1993.
22. Landini G, Rippin JW. Tumour shape and local connected dimension analysis in oral cancer and pre-cancer. In: Novak MM, ed. *Fractal Reviews in the Natural and Applied Sciences. (IFIP Transactions).* London: Chapman & Hall; 1995:171–178.
23. Landini G, Misson GP. Simulation of corneal neovascularization by inverted diffusion limited aggregation. *Invest Ophthalmol Vis Sci.* 1993;34:1872–1875.